Infrared activity of α-$AlPO_4$

J. Camassel and A. Goullet
Groupe d'Etude des Semiconducteurs, Institut de Recherche sur les Matériaux pour l'Electronique, Université des Sciences et Techniques du Languedoc, F-34060 Montpellier Cedex, France

J. Pascual
Departament Física and Institut de Ciencia de Materiales, Universitat Autònoma de Barcelona, E-08193 Bellaterra, Spain

(Received 2 May 1988)

Performing polarized reflectivity and absorption measurements in the experimental range 15–1500 cm^{-1}, we have investigated the infrared activity of phonons in aluminum phosphate. We report both Γ_2 ($\mathbf{E}\|c$) and Γ_3 ($\mathbf{E}\perp c$) polarized components and, in order to identify all modes predicted by group theory arguments, we compare with similar measurements performed on α-quartz. We have found the following. In polarization $\mathbf{E}\|c$, we resolve from reflectivity spectra all but one infrared-active Γ_2 components. Since they are exclusively infrared active, they could not be found from any other technique. To investigate the missing mode, which corresponds to the folded acoustic branch, we performed a series of transmission measurements. In this way we could find a weak absorption structure, which appears at room temperature at 48 cm^{-1}. In polarization $\mathbf{E}\perp c$, we find 15 infrared-active Γ_3 components which compare satisfactorily with previously published Raman data. Two modes, at 112 and 126 cm^{-1}, form a close doublet which resolves only when running absorption measurements at liquid-helium temperature. The high-energy component (126 cm^{-1}) comes from the folded acoustic branch and the second is the infrared counterpart in aluminum phosphate of the 128-cm^{-1} phonon of α-quartz. This is clearly established from a comparison of both reflection and transmission experiments performed on the same sample. Finally, performing a series of oscillator fits, we get quantitative values for (i) the LO-TO splitting of the phonon modes under consideration and (ii) the corresponding oscillator strengths. The series of parameters obtained in this way compare satisfactorily with a simple model of infrared exclusive modes in β-quartz admixed twice: first, with silent or Raman exclusive components (this is the case in the α variety) and, second, with zone-boundary modes (this appears in berlinite when doubling the length of the unit cell).

I. INTRODUCTION

$AlPO_4$ (berlinite) is the prototype member of the family of ternary compounds $A^{(III)}B^{(V)}O_4$ which are isomorphic to quartz. Renewed interest to this class of materials has recently increased[1,2] and follows the use of hydrothermal growth techniques which allow the growth of large single crystals of very homogeneous quality. Because aluminum phosphate exhibits a piezoelectric coupling coefficient larger than quartz and a better thermal stability over a wide range of temperature, it is more and more considered for technical applications. As a matter of fact, on the long-range term, it should compete with quartz in the use and design of volume and surface acoustic wave devices. On a more fundamental viewpoint, whereas the phonon spectrum of α-quartz has been extensively studied in the past by means of spectroscopic techniques like Raman,[3] infrared,[4] or inelastic neutron scattering,[5] not much experimental effort was devoted to the study of phonon spectra in α-quartz isomorphs. Concerning α-$AlPO_4$, only Raman,[1,6,7] together with preliminary infrared measurements,[7,8] and a recent investigation of the hydrostatic pressure dependence of the second-order elastic constants[2] have been reported. Even less information is found about the remaining members of the family.[9]

In this work, we focus on the infrared-active modes of aluminum phosphate. Well polarized reflectivity spectra have been collected at room temperature in the spectral range 15–1500 cm^{-1} and, because the lattice symmetry of berlinite and α-quartz are the same, they have been complemented by identical measurements performed on SiO_2. This follows the path of Jayaraman *et al.*[1] and allows a continuous discussion of data through the series of crystals β-SiO_2 to α-SiO_2 and α-$AlPO_4$, which forms a most interesting family to deal with. Some modes, which are poorly infrared-active, could not be found by simply measuring at room temperature the reflectivity spectra. In this case we had to complement our work by investigating also the infrared absorption spectrum. This permits one to easily identify the two components which are predicted by symmetry considerations and should be associated with the folded acoustic branches. One appears at 48 cm^{-1}, in polarization $\mathbf{E}\|c$, while the second is identified at 126 cm^{-1}, in polarization $\mathbf{E}\perp c$. One point is worth noticing and concerns the latter polarization ($\mathbf{E}\perp c$). A second weak component appears at a slightly lower energy (112 cm^{-1}, at 10 K) and both modes resolve only at low temperature. A close comparison of absorp-

tion and reflection measurements has been performed. It demonstrates that the first one (126 cm^{-1}) does not correspond with the folded acoustic branch (vanishingly small oscillator strength) but rather with the first-order (already weak) 128 cm^{-1} phonon of α-quartz.

From a more quantitative viewpoint, we have performed a series of oscillator fits and deduced experimental values for the LO-TO splitting of all vibrational modes under investigation. In polarization $\mathbf{E}\perp c$, where we could compare with previously published Raman data, we find results in very satisfying agreement. Finally we analyze the corresponding activity in terms of a simple scheme of infrared active modes of β-quartz admixed twice: first, in α-quartz, with former Raman-active components; next, in berlinite, with zone boundary phonons folded to the center of the Brillouin zone. In this way we could compute a series of oscillator strengths in good agreement with the experimental values.

II. CRYSTAL STRUCTURE AND INFRARED ACTIVITY

β-SiO_2 has lattice symmetry D_6 with 3 formula units per unit cell. At the center of the Brillouin zone, the 27 lattice vibrations reduce to 3 acoustic modes, with symmetry $\Gamma_2+\Gamma_5$ (also labeled A_2+E_1 in the literature), and 24 remaining modes with various activities: 5 are silent, with symmetry $3\Gamma_3+2\Gamma_4$ (or $3B_1+2B_2$); 9 are Raman-active [of which 1 is nondegenerate (Γ_1 or A_1) and 4 are 2 times degenerate (Γ_6 or E_2)]; 2 are infrared active in polarization $\mathbf{E}\|c$ (Γ_2 or A_2) and 4 are 2 times degenerate and both Raman and infrared-active in the polarization $\mathbf{E}\perp c$ (Γ_5 or E_1). When reducing the lattice symmetry to α-quartz (D_3), we find again 27 modes of which 3 are acoustic, with symmetry $\Gamma_2+\Gamma_3$ (or A_2+E); 4 are Raman, with symmetry (Γ_1 or A_1); 4 are infrared (Γ_2 or A_2); and, lastly, 8 Γ_3 (or E) modes are, again, 2 times degenerate and both Raman and infrared active. In other words the 5 silent modes of the β modification have been promoted to 3 Raman-active modes, with Γ_1 symmetry, and 2 infrared-active modes, with Γ_2 symmetry. In the same way, concerning the degenerate modes, 4 Raman Γ_6 (or E_2) and 4 Raman and infrared Γ_5 (or E_1) modes in the β-modification couple now in the α variety and become both Raman and ir active. The straightforward consequence is an interplay of Raman cross sections and infrared oscillator strengths for the 8 Γ_3 modes (E_1- or E_2-like modes) of α-quartz with LO-TO splittings depending on the first-order infrared activity. This point, which was first clearly recognized in Ref. 3, rules all aspects of the lattice dynamics of α-quartz and related compounds.

Coming now to α-$AlPO_4$, the lattice symmetry is again D_3 with 3 formula units per unit cell, but now, since there are 2 times more atoms in a formula unit, one expects 54 modes. The group theory predicts at the center of the Brillouin zone: 3 acoustic vibrations ($\Gamma_1+\Gamma_3$); 8 Raman-active modes (with symmetry Γ_1); 9 infrared-active modes (with symmetry Γ_2) and, lastly, 17 Γ_3-modes which are both Raman and infrared active. The point is that the crystal unit cell differs only from α-quartz by the alternate succession of AlO_4 and PO_4 tetrahedra along the c axis, the unit cell being twice as long in this direction. This suggests the use of a "folded-zone" scheme, where all 27 optical "new" modes come directly from the 27 zone-boundary modes of α-quartz with wave vectors $(0,0,\pi/C)$.

Folding the Brillouin zone is a very elegant concept which has proven useful to describe the zone-center phonons of supercell structures and, in this case, folding the phonon branches manifests itself in two different ways.

(i) At low energy, new zone-center modes appear which come directly when folding the acoustic branches. In this work we report for the first time the Γ_2-like mode, appearing in polarization $\mathbf{E}\|c$ at 48 cm^{-1} in aluminum phosphate. As already said, we have found the corresponding oscillator strength to be extremely small and could only resolve this mode by performing transmission experiments to complement our reflectivity spectra.

(ii) At higher energy, satellite structures appear which are related to the "old" optical branches. Of course the correct energy positions depend on the dispersion of the primitive modes and, because berlinite contains 18 atoms per primitive unit cell, it can be viewed as a prototype material which displays a wealth of experimental situations. We have found the following.

First, there are internal vibrations which remember the molecular vibrations of the building units (SiO_4 tetrahedra): They correspond with weak folded modes, very close in energy. This is the typical situation encountered in layered materials which has been mostly used to illustrate the concept of zone folding.

Second, associated with more dispersive optical branches, are ir-active modes in SiO_2 which have no obvious folded replica. This is the case of the 650 cm^{-1} Γ_3 mode ($\mathbf{E}\perp c$). What happens is that the same point group acts at the center of the Brillouin zone and at the critical point A. However, due to difference in phases associated with the fractional lattice translations which take part in

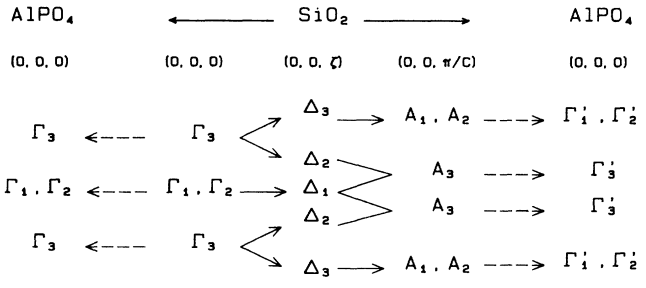

FIG. 1. Interplay of compatibilities between the representations of the symmetry group D_{43} at points $\Gamma(0,0,0)$, $\Delta(0,0,\xi)$ and $A(0,0,\pi/C)$ of the Brillouin zone. Please notice how the two-dimensional representation A_3, at the edge of the Brillouin zone, always combines characters of a one-dimensional representation (Γ_1 or Γ_2) with characters of the two-dimensional representation Γ_3, and vice versa. This means that, in some cases, a one phonon branch must be very dispersive in order that the two modes match at the zone boundary. In this case, no close folded replica can be expected.

TABLE I. Optical activity of phonons in the series β-SiO_2 to α-SiO_2, and α-$AlPO_4$. R (S) stands for a strong, first-order allowed, Raman (infrared) activity. Silent indicates modes which are both Raman and infrared inactive in the β phase. The modes denoted "forb." have wave vector $\mathbf{k}=(0,0,\pi/C)$. The admixture coefficients associated with the β-to-α phase transformation have been denoted α and those corresponding to the doubling of the unit cell have been labeled ϵ. Clearly, two series of folded replicas should be expected for the optical branches and their relative intensities should scale like ϵ and $\alpha\epsilon$, respectively. Lastly, concerning the acoustic branches (acc), one expects again folded replicas and, in both cases, the corresponding activity should be vanishingly small.

SiO_2 (β)		SiO_2 (α)		$AlPO_4$ (α)	
Mode	Activity	Mode	Activity	Mode	Activity
1 Γ_1 (A_1)	R	1 Γ_1 (A_1-like)	R	1 Γ_1 (A_1-like)	R
3 Γ_3 (B_1)	silent	3 Γ_1 (B_1-like)	αR	3 Γ_1 (B_1-like)	αR
		4 A_1 ($k=\pi/C$)	forb.	4 Γ_1' (folded)	$\epsilon R+3\alpha\epsilon R$
2 Γ_2 (A_2)	S	2 Γ_2 (A_2-like)	S	2 Γ_2 (A_2-like)	S
2 Γ_4 (B_2)	silent	2 Γ_2 (B_2-like)	αS	2 Γ_2 (B_2-like)	αS
		4 A_2 ($k=\pi/C$)	forb.	4 Γ_2' (folded)	$2\epsilon S+2\alpha\epsilon S$
4 Γ_5 (E_1)	$R+S$	4 Γ_3 (E_1-like)	$R+S$	4 Γ_3 (E_1-like)	$R+S$
4 Γ_6 (E_2)	R	4 Γ_3 (E_2-like)	$R+\alpha S$	4 Γ_3 (E_2-like)	$R+\alpha S$
		8 A_3 ($k=\pi/C$)	forb.	8 Γ_3' (folded)	$4\epsilon(R+S)$, $4\epsilon(R+\alpha S)$
1 Γ_2 (A_2)	acc.	1 Γ_2 (A_2)	acc.	1 Γ_2 (A_2)	acc.
		1 A_2 ($k=\pi/C$)	forb.	1 Γ_2' (fold-acc.)	(~ 0)
1 Γ_5 (E_1)	acc.	1 Γ_3 (E)	acc.	1 Γ_3 (E)	acc.
		1 A_3 ($k=\pi/C$)	forb	1 Γ_3' (fold-acc.)	(~ 0)

the symmetry elements of this nonisomorphic symmetry group, the correspondence between the 27 normal modes of vibration at A ($4A_1+5A_2+9A_3$) and the 27 modes at $k=0$ is not straightforward. To make this point clear, we list in Fig. 1 the compatibility relations between points $k=0$ and $k=(0,0,\pi/C)$ in SiO_2. Notice that, every time, Γ_3 breaks into two one-dimensional representations ($\Delta_2+\Delta_3$) while the two-dimensional representation A_3 is only compatible with both one branch issued from Γ_3 (Δ_2) and one branch issued from Γ_1 or Γ_2 (Δ_1). This means that, in some cases, the phonon branches must be very dispersive in order that two branches match at the zone boundary and, in this case, no close folded replica should be expected. Moreover, depending on the activity of the zone-center mode (Γ_1 or Γ_2) the replica can exhibit more Raman than infrared activity.

Third, we have found that, in some cases, a resonant coupling occurs between a zone-center phonon and a folded mode of identical symmetry which appears at about the same energy. In this case there is a large transfer of oscillator strength which results in the enhanced activity of the folded mode. This is the case of the 440 cm^{-1} Γ_2' mode in polarization $\mathbf{E}\|c$.

Fourth, when two modes have crossed and decouple again, they have exchanged their energy positions but retain their own activity. This is the case of the 112–126-cm^{-1} Γ_3 doublet, in polarization $\mathbf{E}\perp c$ at 10 K. The first component corresponds with the weak 128-cm^{-1} mode of α-quartz and the second with the folded acoustic branch. This is the one which corresponds with the smallest (vanishingly small) oscillator strength.

Concerning now the relative intensities, in the limiting case where the two Al and P atoms were replaced by silicon, the supercell would vanish. Indeed, if we just fold the Brillouin zone of α-SiO_2 at point $(0,0,\pi/2C)$, 27 new (fictive) Γ' modes appear which are all in fact optically inactive. This is because the like atoms, in the two sublattices which form the supercell, vibrate in opposite phases and cancel the resulting polarizability. On the other hand, in a real ternary crystal of $AlPO_4$, the ancient A-like modes become true Γ ones and the relative strength of the new "folded" modes is a measure of how far the chemical bonding is changed. In Table I, we summarize the activity of phonons through the sequence β-SiO_2 to α-SiO_2 and α-$AlPO_4$. First there appears an admixture coefficient α which describes the infrared activity induced by distorting the structure from D_6 to D_3 (β-to-α transition). As will be evidenced when discussing the experimental data, this defines two classes of structures. Next appears an admixture coefficient ϵ which describes the change in bonding properties between silicon, on the one hand, and aluminum or phosphorus, on the other hand. Since Al, Si, and P are as close as possible on the Periodic Table, one expects in our case weak "folded" Γ'-like replicas and previous Raman investigations[6] support this expectation.

III. EXPERIMENTAL DETAILS

We have used a Brucker IFS, far-infrared Fourier transform, spectrometer,[10] fitted with standard pyroelectric detectors in the spectral range 250–1500 cm^{-1}. In the range 15–250 cm^{-1}, two different bolometers were used and cooled down to pumped liquid-helium temperature to achieve a maximum signal-to-noise ratio. The nominal resolution was typically 4 cm^{-1} and from 50 to 250 scans were done in order to average the data.

The samples used in this work have been grown by J.

C. Jumas and E. Philippot, from the Institut de Recherche sur les Matériaux pour l'Electronique (IRME), using a hydrothermal growth technique. They had a slightly trapezoidal shape, with typical thicknesses $e=1$ mm, and were cut from large single crystals. In order to get the best polarized data, we identified first the a and c axes in the large faces of the sample and, second, used rotating polarizers in order to adjust exactly from sample to sample. Two different series of polarizers have been used and covered the whole experimental range. When necessary the samples were mounted inside a liquid-helium cryostat and cooled down to about 10 K using an exchange gas technique. In this configuration only the transmission spectra could be investigated.

IV. EXPERIMENTAL RESULTS

A. Γ_2 modes (E$\|c$)

Figure 2 summarizes most of our experimental findings in polarization E$\|c$. Consider first SiO_2 [see Fig. 2(a) and the transverse phonon frequencies listed in Table II]. First are two strong reflectivity features at 495 and 1080 cm^{-1}. They dominate the spectrum and identify the two

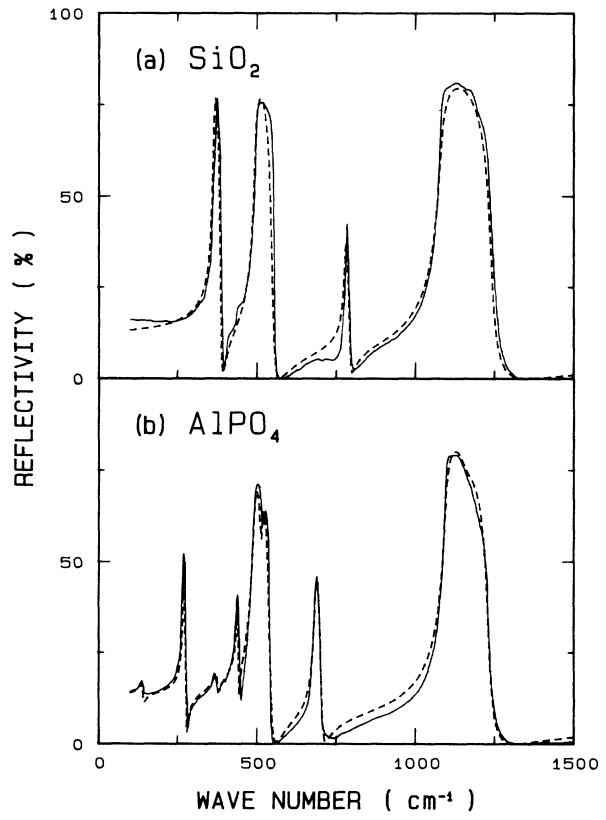

FIG. 2. Reflectivity spectra of both (a) SiO_2 and (b) $AlPO_4$ in polarization E$\|c$ (Γ_2 modes). Notice the strong (A_2-like) components which dominate the spectra. They come from the first-order infrared-active frequencies of β-quartz and are associated with internal vibrations of the building units. Dashed curves are oscillator fits to the experimental data (solid lines).

infrared-active (A_2-like) components of β-quartz. Next come two modes, at 364 and 780 cm^{-1}, which originate from the silent B_2-like vibrations promoted to A_2 symmetry in the α variety. All will be, of course, first-order components of the infrared reflectivity spectrum of α-$AlPO_4$, but we see immediately that they will be associated with different activities. Concerning their relative identification in terms of atomic displacements we know, from simple calculations which take only into account central force constants between neighboring atoms,[11] that all silicate groups should exhibit two series of nearly degenerate Raman and infrared bands associated with the triply degenerated Γ_5 (T_2) states of the tetrahedron. This is not only true for crystals but also for molecules.[12] In the remaining part of this work, the corresponding vibrations will be mainly referred to as molecular (or intratetrahedral) vibrations. Their relative energy positions can be easily obtained from the simplest model of axially symmetric tensor forces between neighboring atoms. The potential energy between two silicon and oxygen atoms can be written in this case:

$$\Phi_i=\lambda_i/r_i^n ,$$

where $i=1$ accounts for first-nearest-neighbor distance and n should be of the order of 5 for a typical oxide.[13] This results in two bond stretching and bond bending constants:

$$A_i=n(n+1)\lambda_i/r_i^{n+2}$$

and

$$B_i=n\lambda_i/r_i^{n+2} .$$

The important point to notice is that both are in a typical ratio $(n+1)$ which, in this case, is of the order of 6. Since hydrostatic pressure experiments[14] effectively demonstrate that the high-energy component (1080 cm^{-1}) corresponds with internal stretching vibrations, we expect the corresponding bending vibration to fall at about 450 cm^{-1}. This is in quite good agreement with the experimental value (495 cm^{-1}) and, since both modes behave like internal modes, they are not expected to change when going from SiO_2 to $AlPO_4$. We shall see later that this is indeed what is found.

The first B_2-like mode appears at 780 cm^{-1}. This is the so-called ring mode which occurs when there is both a ring-forming connection and intertetrahedral interactions. Since, on the microscopic scale, it connects directly with oxygen-oxygen interactions, it should be very sensitive to the detail of the crystal structure. Indeed, it was infrared inactive in the β modification and, as we shall see, shifts from 780 to 684 cm^{-1} when going from SiO_2 to $AlPO_4$. Assuming again a main stretching character, we expect the corresponding bending vibration to fall at about 320 cm^{-1} in SiO_2. This is in rather good agreement with the energy position of the second B_2-like mode [which appears at 364 cm^{-1} in Fig. 2(a)] and confirms, on a rather qualitative viewpoint, the microscopic nature of these interactions. Concerning now the relative oscillator strength of the A_2-like (silicon-oxygen) and B_2-like (oxygen-oxygen) components, it is interesting to point out

TABLE II. (a) Summary of experimental values obtained in this work for the Γ_2 modes of α-SiO_2. We have listed both longitudinal and transverse frequencies (see text). Also listed are (b) the results of Ref. 4 and (c) a theoretical estimate of oscillator strength. * indicates input parameters, and given in parentheses are combination and/or sample-dependent features.

	Γ_2 modes (cm^{-1})			Oscillator fit parameters				
	TO		LO	S			Γ	
	(a)	(b)	(a)	(a)	(b)	(c)	(a)	(b)
B_2-like	364	364	387	0.68	0.68	0.7*	0.014	0.014
A_2-like	495	495	550	0.70	0.66	0.7	0.020	0.009
Sample dependent		(509)			(0.05)			(0.014)
Combination		(539)			(0.006)			(0.04)
B_2-like	780	778	795	0.11	0.10	0.04	0.012	0.010
A_2-like	1080	1080	1240	0.67	0.67	0.7	0.020	0.007
Combination		(1220)			(0.011)			(0.15)

from Table I that they should be simply related by one single parameter α. It describes the averaged coupling when going from the β to α modifications. At first glance this parameter α should be only dependent on the lattice distortion. In fact, since it relies on basically identical interactions, we have found that it is roughly speaking the same whether the activity is induced through β-to-α distortion in polarization $\mathbf{E}\|c$ or through direct ring-forming effects in polarization $\mathbf{E}\perp c$. We shall come back to this point later when quantitatively analyzing the data.

Coming now to aluminum phosphate, a complete reflectivity spectrum is displayed in Fig. 2(b) and the corresponding infrared frequencies have been listed in Table III. One expected 9 Γ_2 modes but we could only resolve 8 reflectivity structures. They appear at 140, 270, 375, 440, 490, 515, 684, and 1095 cm^{-1}. Comparing with the work of Ref. 7, we find a good overall agreement with two exceptions at 375 and 515 cm^{-1}. Both features seem to be sample dependent and behave like a very sharp structure, observed at 509 cm^{-1} in SiO_2 (see Ref. 4). Similar discrepancies have been reported for SiC and GaP (Ref. 15) and indicate extrinsic effects. As a direct consequence only six Γ_2 modes, of which the TO frequencies are 140, 270, 440, 490, 684, and 1095 cm^{-1}, will be considered further. In close agreement with the SiO_2 data, two A_2-like modes dominate the spectrum. As already said, we did not expect their energy to shift much when going from α-quartz to aluminum phosphate and this is indeed what is found. They were listed at 495 and 1080 cm^{-1} in Table II and appear now at 490 and 1095 cm^{-1}, respectively.

The first B_2-like mode appears at 684 cm^{-1}. It is very similar in shape to the structure observed at 780 cm^{-1} in SiO_2 but is shifted down by about 100 cm^{-1}. This confirms the extreme sensitivity to the details of the crystal structure already noticed. The second B_2-like mode should be identified next. It corresponded in α-quartz to the sharp reflectivity structure found at 364 cm^{-1} [see Fig. 1(a)] and, coming back to our simple model of bond-stretching and bond-bending force constants but starting now from the experimental value $\nu=684$ cm^{-1}, we expect it to fall in aluminum phosphate at about 280 cm^{-1}. This corresponds well with the sharp reflectivity structure found at about 270 cm^{-1} and, again, corroborates a shift of 100 cm^{-1}.

TABLE III. Same as Table II, but for α-$AlPO_4$. (a) This work. Except the weak 48-cm^{-1} mode, all phonon frequencies have been obtained from reflectivity measurements and oscillator fit parameters. (b) Reference 7. In this case a small feature was identified at 680 cm^{-1} which was not found in our work. (c) Theoretical estimates using $\alpha_1=8\times10^4$ cm^{-2} and $\epsilon=1.4\times10^4$ cm^{-2}.

	Γ_2 modes (cm^{-1})				Oscillator fit parameters				
	TO		LO		S			Γ	
	(a)	(b)	(a)	(b)	(a)	(b)	(c)	(a)	(b)
Γ_2' (acoustic)	48		48		4×10^{-3}		0.8	0.02	
Γ_2'-like	140		140		0.10		0.15	0.060	
B_2-like	270	273	275	287	0.23	0.495	0.58	0.011	0.029
Sample dependent	(375)		(375)		(0.04)			(0.020)	
Γ_2'-like	440	450	446	457	0.10	0.288	0.09	0.008	0.021
A_2-like	490	494	544	556	0.77	0.783	0.7	0.025	0.024
Sample dependent	(515)		(518)		(0.03)			(0.018)	
Γ_2'-like		(680)		(681)		(0.034)			(0.019)
B_2-like	684	688	705	713	0.17	0.143	0.07	0.016	0.017
A_2-like	1095	1101	1230	1256	0.60	0.571	0.7	0.015	0.009
Γ_2'-like	1160	1158	1160	1154	0.010	0.027	0.007	0.050	0.084

The four structures identified up to now were first-order components of the infrared reflectivity spectrum of $AlPO_4$ and we are now looking for folded replicas. Consider first the A_2-like modes. Owing to the large molecular character of the vibrations, one expects almost dispersionless branches and closely folded Γ'-like partners. This is indeed what happens. At higher energy, one mode which is not experimentally resolved results in the asymmetric line shape of the high-energy component. From the line fitting procedure (see discussion) we find the corresponding transverse frequency at 1160 cm^{-1}. The second one appears at 440 cm^{-1} and has a strong activity which comes from a resonant coupling with the first-order modes. Let us call $|\Gamma_2\rangle$ and $|A_2\rangle$ the corresponding wave vectors, $\omega_0^2(\Gamma)$ and $\omega_0^2(A)$ the eigenstates, and $\langle\Gamma_2|D'|A_2\rangle$ the perturbation matrix element of the dynamical matrix which appears when going from SiO_2 to $AlPO_4$. We get from standard perturbation theory

$$\omega^2(\Gamma_2)=\omega_0^2(\Gamma_2)+\langle\Gamma_2|D'|\Gamma_2\rangle+\frac{|\langle\Gamma_2|D'|A_2\rangle|^2}{\omega_0^2(\Gamma_2)-\omega_0^2(A_2)} \tag{1}$$

and

$$\omega^2(\Gamma_2')=\omega_0^2(A_2)+\langle A_2|D'|A_2\rangle+\frac{|\langle A_2|D'|\Gamma_2\rangle|^2}{\omega_0^2(A_2)-\omega_0^2(\Gamma_2)}\ , \tag{2}$$

where the first-order (diagonal) perturbation matrix elements correspond to a simple renormalization of the SiO_2-like states. This renormalization is weak for internal modes and large (~ 100 cm^{-1}) for structure sensitive oxygen-oxygen interactions but, in both cases, it does not change the symmetry of the wave function. In other words it cannot render active any folded replica. This activity comes only from the second-order terms and all new eigenstates must be written

$$|\Gamma_2\rangle=|\Gamma_2\rangle+\frac{\langle\Gamma_2|D'|A_2\rangle}{\omega_0^2(\Gamma_2)-\omega_0^2(A_2)}|A_2\rangle \tag{3}$$

and

$$|\Gamma_2'\rangle=|A_2\rangle+\frac{\langle A_2|D'|\Gamma_2\rangle}{\omega_0^2(A_2)-\omega_0^2(\Gamma_2)}|\Gamma_2\rangle\ . \tag{4}$$

It is the admixture coefficients $\langle A_2|D'|\Gamma_2\rangle$ which makes an old zone-boundary mode infrared active in aluminum phosphate. It is generally small but, depending on the difference in original frequencies, one can get more or less resonance effect and resulting activity. We shall be more quantitative when analyzing the data.

Consider now what happens when folding the B_2-like components. One point is clear and concerns the weak structure found at 140 cm^{-1}: It comes from the 270 cm^{-1} B_2-like mode, taking account of the rather large dispersion which affects the low-frequency Δ_3 components. In contrast the folded replica of the second B_2-like mode at 684 cm^{-1} is missing. This is a point worth mentioning since the theoretical calculation[16] predicts a close replica (within about 14 cm^{-1}) and the authors of Ref. 7 identified a small component at 680 cm^{-1} (see Table III). In this work, despite a careful examination of the experimental spectra, we cannot confirm this identification. In Fig. 2(b) we notice of course an asymmetrical line shape in this frequency range but a similar behavior appears in α-quartz. Since, in this case, it was assigned to combination bands,[4] we have found it quite impossible to discriminate between the two different contributions.

Finally we focus on the Γ_2'-like mode associated with the folded low-frequency acoustic branches. From neutron scattering experiments performed on SiO_2,[5] one predicts a value of 52 cm^{-1} which has never been checked before and differs significantly from the theoretical estimates (see again Ref. 16). In this work we have undertaken a careful investigation of the experimental reflectivity spectrum from 15 to 100 cm^{-1} and could not identify any clear structure. The only way to get conclusive data was by running transmission experiments through a fairly large piece of crystal (about 5 mm thick). Polarizing $\mathbf{E}\|c$, we could resolve a clear transmission deep at 48 cm^{-1}

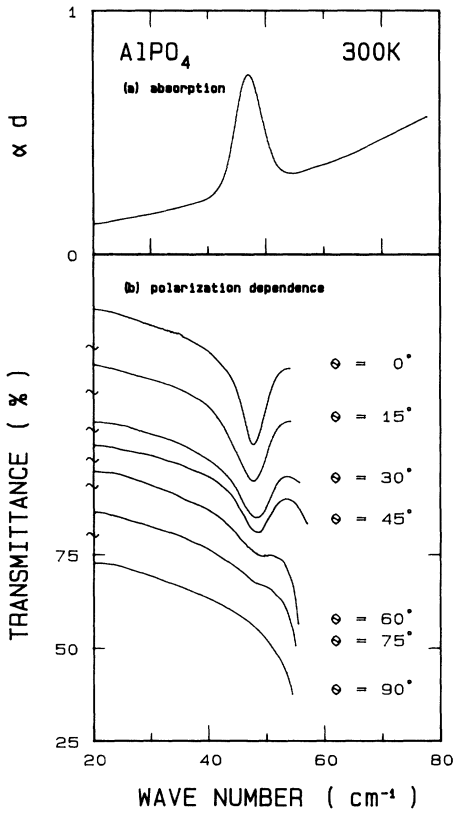

FIG. 3. (a) Absorption peak observed at 48 cm^{-1} (300 K) in polarization $\mathbf{E}\|c$. (b) Polarization dependence observed at 300 K. The experimental absorption curves have been shifted down for clarity and range from $\phi=0$ ($\mathbf{E}\|c$) to $\phi=90°$ ($\mathbf{E}\perp c$).

which disappears in polarization $\mathbf{E} \perp c$. This is shown in Fig. 3. The corresponding oscillator strength, which is obviously very small, prevents any observation by any conventional reflectivity technique.

To summarize, we expected 9 Γ_2 modes from symmetry considerations but could only resolve 7 by performing infrared reflectivity and transmission measurements. An eighth mode will be deduced from the oscillator fit and the last one is missing. Lastly, two extra features which appear on the experimental spectra will be included in the theoretical analysis but should not be considered as first-order components of the intrinsic spectrum of aluminum phosphate in polarization $\mathbf{E} \| c$.

B. Γ_3 modes ($\mathbf{E} \perp c$)

Coming now to the Γ_3 modes, we display a first series of polarized reflectivity spectra in Fig. 4. They correspond to the experimental range 150–1500 cm^{-1}. In both cases, no infrared-active mode with Γ_3 symmetry could be identified below 150 cm^{-1} using conventional pyroelectric detectors.

Consider first α-quartz. One expects 8 infrared-active modes with mainly two series of different oscillator strengths. First, four modes originate from the E_1 modes of β-quartz where they are both Raman and infrared active: They should have a quite large oscillator strength. Second, four modes originate from the Raman exclusive E_2 modes of β-quartz: They should be associated with a much smaller activity. In fact, the experimental results depart from this simple picture. We could only resolve 7 modes, of which only three are clearly identified. Two are strong E_1-like components [see Fig. 4(a) and Table IV] and appear at 452 and 1072 cm^{-1}. Those are the ones which are clearly associated with internal (intratetrahedral) vibrations. The third one is an old Raman partner which has an E_2-like character: It appears at 1162 cm^{-1}. The remaining four modes, which are found at 265, 396, 699, and 799 cm^{-1} correlate with the ring-forming connection (intertetrahedral or oxygen-oxygen interactions). They are more difficult to assign. On the basis of both infrared intensities and Raman scattering experiments,[3,17] one associates the E_1-like character with the large reflectivity structure found at 799 cm^{-1}; the other ones are E_2-like components. One E_1-like mode is missing. Concerning now the relative intensities, we notice that the infrared oscillator strengths are very close to the one observed for the Γ_2-like modes in polarization $\mathbf{E} \| c$ [see Fig. 2(a)]. This indicates that, roughly speaking, the same matrix element α couples molecular (intra-

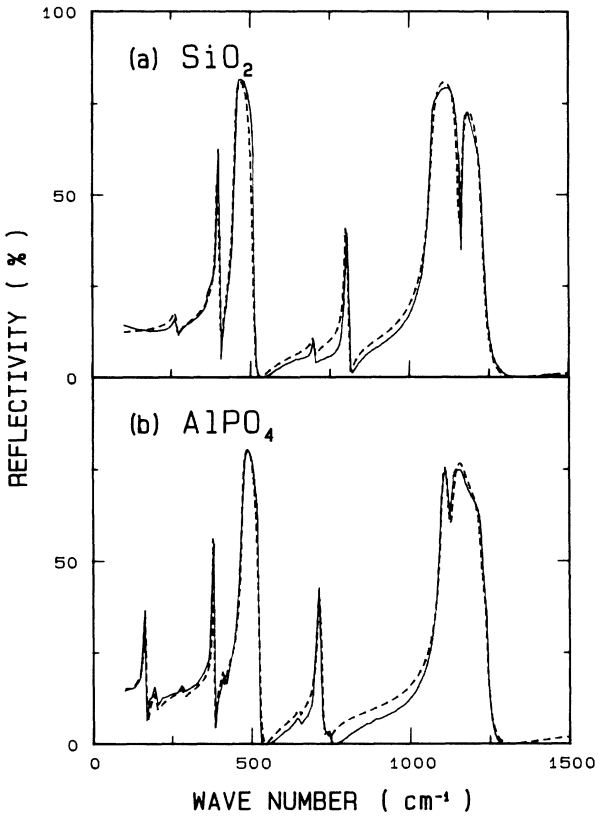

FIG. 4. Same as Fig. 2 in polarization $\mathbf{E} \perp c$. Four E_1-like modes are first-order infrared active and should dominate the spectra. In fact both α-quartz and aluminum phosphate, exhibit only two strong (internal or molecular) modes. All other frequencies have much weaker activity and can be described in terms of successive perturbations. See text.

TABLE IV. (a) Summary of the relevant parameters obtained in this work for the Γ_3 modes of α-SiO_2. Also listed are the results of (b) Ref. 4 and (c) Ref. 3. In both cases (a) and (c), we give longitudinal and transverse phonon frequencies; (d) gives a theoretical estimate of oscillator strengths according to the simple model discussed in the text. * indicates input parameters.

	Γ_3 modes (cm^{-1})					Oscillator fit parameters				
	TO			LO		S			Γ	
	(a)	(b)	(c)	(a)	(c)	(a)	(b)	(d)	(a)	(b)
E_1-like	128		128	128	128					
E_2-like	265		265	265	265	0.080		0.2	0.040	
E_2-like	396	394	394	405	401	0.31	0.33	0.3*	0.011	0.007
E_1-like	452	450	450	510	509	0.77	0.82	0.7	0.018	0.009
E_2-like	699	697	697	699	697	0.015	0.018	0.07	0.012	0.012
E_1-like	799	797	795	810	807	0.095	0.11	0.04	0.009	0.009
E_1-like	1072	1072	1072	1230	1235	0.63	0.67	0.7	0.016	0.007
E_2-like	1162	1163	1162	1156	1162	0.018	0.010	0.011	0.014	0.006
		(1227)					(0.009)			(0.11)

tetrahedral) and crystalline (intertetrahedral) modes independently of the details of the coupling mechanism.

Our results should be compared with the work of Ref. 4 where only 6 clearly resolved one-phonon modes have been found. We could resolve an additional structure (E_2-like mode) at 265 cm^{-1} but, in both cases, the first E_1-like component was missing. As already said, it is known to appear around 128 cm^{-1} (see for instance the polarized Raman data of both Refs. 3 and 17) but was also observed in the far-infrared region using the asymmetric Fourier-transform method.[18] In order to get a reference spectrum, to compare with in aluminum phosphate, we decided to complement our data. We have investigated the transmission spectrum of a rather thick piece of crystal, in polarization E⊥c, and could resolve the small absorption feature displayed in Fig. 5. This corresponds satisfactorily with the results of Ref. 18.

Coming now to aluminum phosphate, we expected to find 17 Γ_3 modes. From the room-temperature reflectivity data displayed in Fig. 4(b), together with the oscillator fit analysis discussed in the next section, we hardly resolve more than 13 infrared active components. For convenience they have been listed in Table V.

At high energy, four modes range from 1100 to 1228 cm^{-1}. They come from the high-energy structures (E_1- and E_2-like modes) of α-quartz and only three (1100, 1130, and 1180 cm^{-1}) were experimentally resolved. The last one (1228 cm^{-1}) comes from the line fitting procedure.

Three modes range between 650 and 738 cm^{-1}. They come in various ways from the structure sensitive oxygen-oxygen interactions. With respect to α-quartz, we first notice a downshift by about 100 cm^{-1} which closely parallels the results obtained in polarization E‖c for the corresponding vibrations. We notice also that the

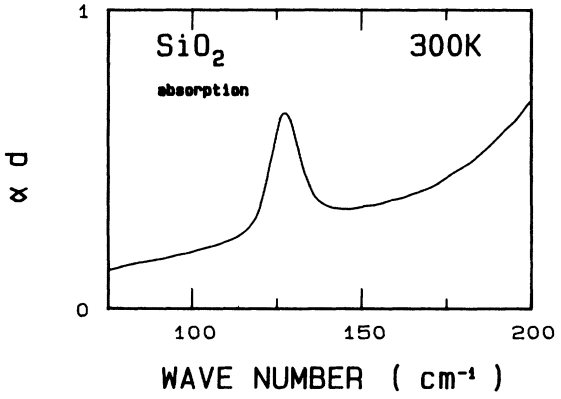

FIG. 5. Absorption spectrum corresponding to the 128-cm^{-1} Γ_3 mode of α-quartz. Up to now the corresponding vibration was mostly identified in Raman experiments.

dispersion of the various components reflects the dispersion of the theoretical curves (see for instance Ref. 16). This indicates (i) that the mode at 738 cm^{-1} is the folded replica of the first-order one observed at 710 cm^{-1} (E_1-like vibration), and (ii) that the folded component of the 650 cm^{-1} (E_2-like) mode is not experimentally found. As already said, the reason lies in the details of the microscopic structure of α-quartz and the resulting lattice dynamics. Indeed, since any folded frequency with Γ_3 symmetry comes from the Δ_2 singlet branch of a degenerate Γ_3 mode admixed with a Δ_1 branch (see Fig. 1), it has to match a Γ_1 or Γ_2 zone-center phonon. In some cases, see again Ref. 16, the theoretical estimates predict that there should be a strong dispersion of the phonon branches in

TABLE V. Same as Table IV, but for aluminum phosphate (α phase). (a) This work. Two frequencies marked by subindex t have been obtained from transmission experiments performed at 10 K. (b) Reference 7 (infrared data); (c) Ref. 7 (Raman data); (d) Ref. 6; (e) theoretical estimate (see text). Given in square brackets are poorly resolved LO components (see Ref. 7).

	Γ_3 modes (cm^{-1})								Oscillator fit parameters				
	TO				LO				S			Γ	
	(a)	(b)	(c)	(d)	(a)	(b)	(c)	(d)	(a)	(b)	(e)	(a)	(b)
E_1-like	$(112)_t$		104	105	$(112)_t$			105					
Γ_3' (acoustic)	$(126)_t$		115	116	$(126)_t$			116					
E_2-like	165		160		170				0.31		0.19	0.031	
Γ_3'-like	198		193	192	205			192	0.10		0.21	0.07	
Γ_3'-like	285		305	296	286			296	0.03		0.04	0.04	
E_2-like	379	378	371	371	385	390	382	378	0.132	0.329	0.126	6×10^{-3}	0.022
Γ_3'-like	414	418	417	417	415	419	[418]	436	0.018	0.034	0.099	6×10^{-3}	0.022
Γ_3'-like		448	437			449	[438]			0.018	0.19	0.03	0.022
E_1-like	473	468	463	460	525	523	522	568	0.80	0.733	0.7	0.017	0.018
Γ_3'-like			565				[568]						
E_2-like	650	646	650	697	650	647	[650]	697	0.004	0.009	0.015	0.005	0.025
E_1-like	710	705	703	713	725	724	721	713	0.13	0.143	0.05	0.014	0.017
Γ_3'-like	738	747	748		738	749			0.007	0.010	0.007	0.013	0.015
E_1-like	1100	1101	1102	1100	1240	1247	1239	1239	0.48	0.497	0.7	0.01	0.008
E_2-like	1130	1130		1130	1125	1127		1125	0.098	0.043	0.106	0.02	0.015
Γ_3'-like	1180	1186	1198		1180	1186	1198		0.010	0.006	0.005	0.05	0.034
Γ_3'-like	1228	1229	1228	1231	1228	1224	1228	1231	0.0005	0.003	0.0017	0.01	0.065

order that they can effectively match. In this case the infrared activity associated with the Γ_3 mode might be lost and the folded replica would appear like the zone center mode. For instance a Γ_1 mode would induce a preferential Raman activity and a Γ_2 mode a more infrared active replica. Concerning the 650 cm^{-1} zone-center mode, the "folded frequency" is predicted at about 560 cm^{-1} and we believe that the infrared activity is lost. The corresponding Γ'-like mode, which is not found in this work, appears in Raman spectroscopy (see Table V).

Next comes a series of six modes, ranging from 165 to 473 cm^{-1}, whose tentative assignment is given in Table V. The only clearly identified modes are, first, the E_1-like components at 473 and 379 cm^{-1} and, second, the E_2-like one at 379 and 165 cm^{-1}. Weaker structures at 198, 285, and 414 cm^{-1} are folded replicas.

Again three frequencies are missing. From the Raman data listed in Table V, one expects the first one to fall at about 440 cm^{-1}. Despite a careful search in this energy range, and for similar reasons to the one discussed for the 650 cm^{-1} E_2-like mode, we could not resolve it. The two other ones correspond to the low-frequency (infrared active) components reported around 100 cm^{-1} in Raman scattering experiments. An experimental evidence of these structures was found from the transmission spectra reported in Fig. 3(b) (polarization dependence): We find a clear cutoff which develops (starting from about 50 cm^{-1}) when shifting from $\mathbf{E}\|c$ to $\mathbf{E}\perp c$. It corresponds with the appearance of the first Raman-active Γ_3 mode. This increased experimental absorption corresponds with the threshold of a Raman doublet, resolved at 105–116 cm^{-1} in Ref. 6 and 104–115 cm^{-1} in Ref. 7, respectively. To complement our data, we have again investigated the transmission spectrum of our sample in this energy range. It was kept at 10 K in a liquid-helium cryostat, equipped with Mylar windows, and the detector was a Ge bolometer cooled down to about 1.6 K. The resulting spectrum, obtained when using unpolarized light, is shown in Fig. 6(a). We resolve two peaks, at 112 and 126 cm^{-1}, which normally should correspond with, first, the folded acoustic branch, and second, the 128-cm^{-1} (E_2-like) mode of α-quartz. This is the standard ordering that one expects. However the larger oscillator strength found for the first structure questions this natural ordering. To make this point clear, we have investigated (using the same sensitive detector) the room-temperature reflectivity spectrum of our sample. The resulting data are shown in Fig. 6(b). Only one structure appears at room temperature in this energy range. It is weak and corresponds with the 112-cm^{-1} feature. The Γ_3-like character is clear and demonstrated from the polarized spectra displayed in Fig. 7. Nothing appears at 126 cm^{-1}. This demonstrates the

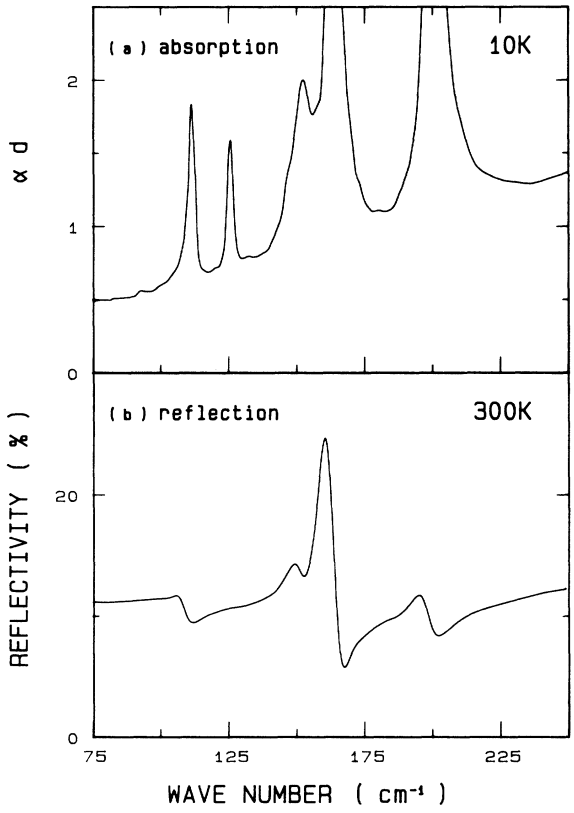

FIG. 6. Comparison of (a) the low-temperature (10 K) transmission spectrum of a thick piece of aluminum phosphate, and (b) the room-temperature reflectivity spectrum. In both cases a larger structure is found around 112 cm^{-1}.

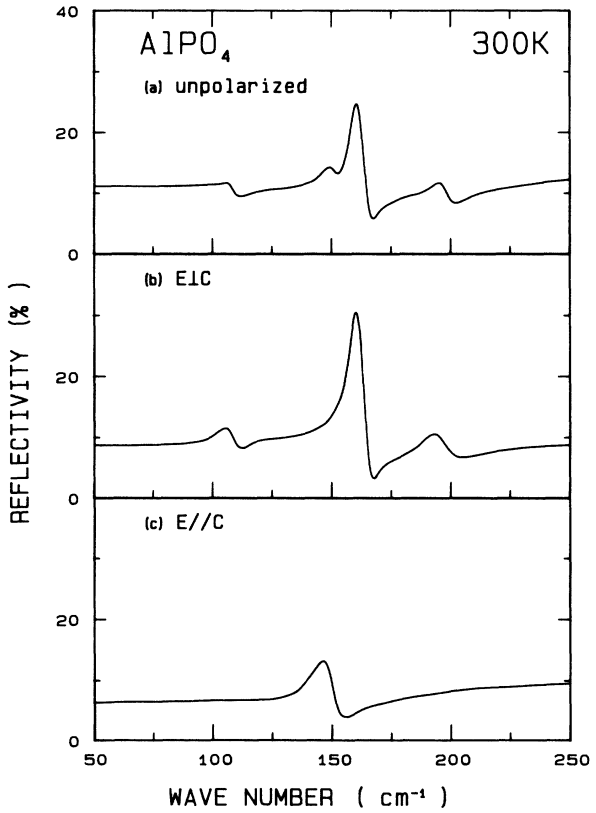

FIG. 7. Polarization dependence of the room-temperature reflectivity spectrum of Fig. 5. Notice the Γ_3 character of the first structure (112 cm^{-1} at 10 K) while nothing is revealed near 126 cm^{-1} (vanishing oscillator strength).

vanishingly small oscillator strength and the folded-acoustic-like character of this vibration.

To summarize, from symmetry considerations we expected 17 Γ_3 modes but could only resolve 15. The two modes, which are missing from our infrared investigations, have been only reported using Raman techniques. They correspond with dispersive Δ_2 branches matching a Δ_1 branch issued from a first-order Raman active mode.

V. OSCILLATOR FIT ANALYSIS

We have performed a series of oscillator fits to the experimental data in order to determine precisely all phonon frequencies and oscillator strengths which participate in the reflectivity spectra. A standard expression for the complex dielectric constant has been used:

$$\epsilon(\nu)=\epsilon_\infty+\sum_j \frac{S_j\nu_j^2}{(\nu_j^2-\nu^2)+i\Gamma_j\nu_j\nu}\ , \tag{5}$$

where ϵ_∞ accounts for the electronic contribution, S_j is a reduced, dimensionless, oscillator strength, Γ_j is a reduced damping parameter, and ν_j is the phonon wavenumber. The results are shown as dotted lines in Figs. 2 and 4, while the parameters are listed in Tables II–V. Also listed for comparison purpose are the infrared results given by Spitzer *et al.*[4] for α-SiO_2, Lazarev *et al.*[7] for α-$AlPO_4$ in the range 300–1200 cm^{-1}, and the Raman data[6,7] collected in Γ_3 ($\mathbf{E}\perp c$) configuration for both series of compounds. Since the Raman data are sensitive to the longitudinal or transverse nature of the phonon mode under investigation, we have deduced LO-TO splitting values from our infrared data by plotting both $\mathrm{Im}(\epsilon)$ and $\mathrm{Im}(-1/\epsilon)$ on the same graph. This is shown in Fig. 8, for the polarization $\mathbf{E}\|c$, and Fig. 9, for the polarization $\mathbf{E}\perp c$. The important point to notice is that, while the imaginary part of the dielectric function exhibits its maximum values which peak at the transverse phonon frequencies, the loss function $[\mathrm{Im}(-1/\epsilon)]$ peaks at the longitudinal phonon frequencies. In other words the simple consideration of Figs. 8 and 9 illustrates the magnitude of the LO-TO splitting for all phonon modes under investigation and should directly correlate with the infrared activity.

Consider first SiO_2. In polarization $\mathbf{E}\|c$, all TO frequencies obtained in our work are in good agreement with the results of Ref. 4. The main difference, however, is that, besides the four fundamental one-phonon modes predicted by the group theory, three additional resonances were introduced in Ref. 4. They were assigned to combination bands and, of course, this resulted in a much better oscillator fit which has not been reproduced here. From a consideration of both Fig. 7(a) and Table II, we find a magnitude of the LO-TO splitting which correlates directly with the oscillator strength and confirms the A_2-

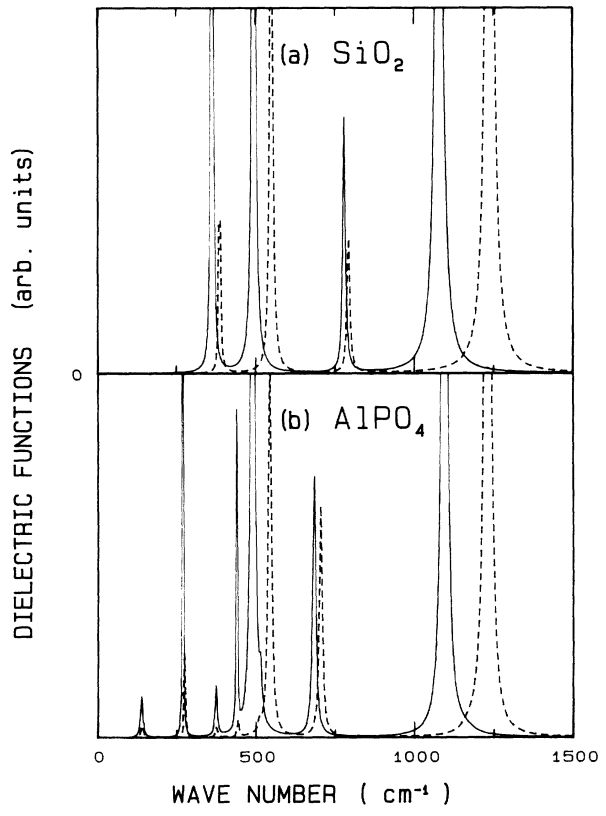

FIG. 8. Comparison of the theoretical dispersion computed in polarization $\mathbf{E}\|c$ for the two dielectric functions $\mathrm{Im}(\epsilon)$, solid lines, and $\mathrm{Im}(-1/\epsilon)$, dotted lines. (a) SiO_2 and (b) $AlPO_4$.

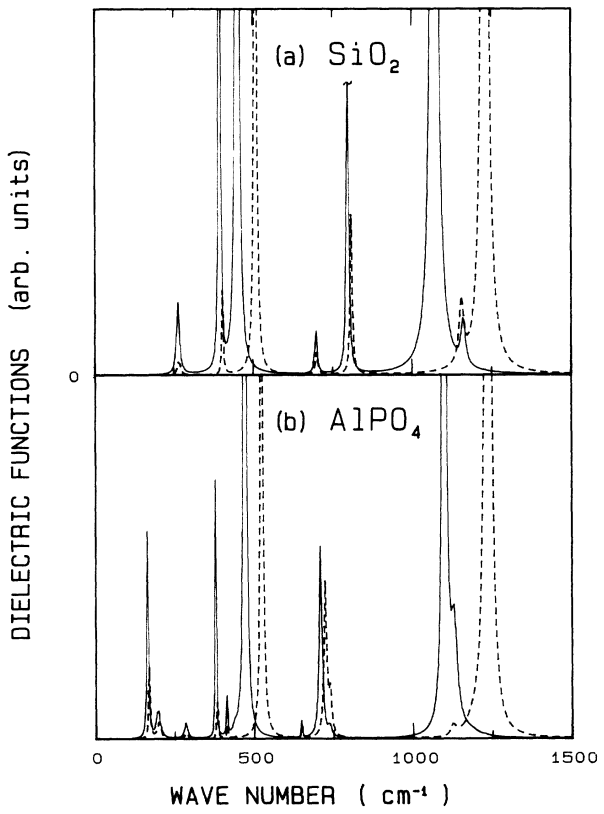

FIG. 9. Same as Fig. 8 in polarization $\mathbf{E}\perp c$.

and B_2-like character of the four phonon modes under consideration. Since these results confirm the large dispersion of oscillator strength which exists between first-order allowed (A_2-like) and first-order forbidden (B_2-like) infrared-active components, we have found it interesting to check how well a simple model could account for the dispersion of the experimental results through the complete family. We use one single average matrix element α_1 to account for the coupling of allowed-to-forbidden vibrational modes ($\mathbf{E}\|c$) in the β-to-α phase transformation and consider only a constant value $S=0.7$ for the molecular first-order oscillator strength through the entire family. In this case we start from a generalization of Eq. 4 and express the "forbidden" oscillator strength $S(\Gamma_j')$ as

$$S(\Gamma_j')=\frac{1}{\omega_j^2}\sum_i \frac{\alpha^2}{(\omega_j^2-\omega_i^2)^2}\omega_i^2 S(\Gamma_i)\ . \tag{6}$$

From the activity ($S=0.68$) of the first B_2-like mode (364 cm^{-1}), we determine $\alpha_1=8\times10^4$ cm^{-2}. Next we compute $S=0.04$ for the second (780 cm^{-1}) B_2-like component. This is rather close to the experimental value ($S=0.11$) and indicates that the simple consideration of a few "averaged" perturbation matrix elements of the dynamical matrix should permit one to account for most of the relative changes in intensity through the sequence β-SiO_2 to α-SiO_2 and α-$AlPO_4$.

Coming now to the Γ_3 modes ($\mathbf{E}\perp c$), a summary of our experimental results is given in Table IV and compared with previously published data. Again the LO frequencies are obtained from a plot of $\mathrm{Im}(-1/\epsilon)$ and the magnitude of the LO-TO splitting illustrated in Fig. 9(a). As already said, two classes of E_1-like modes exist. One comes from the "molecular" Si-O interactions and the second from the "crystalline" O-O interactions. Now the experimental results suggest that, roughly speaking, identical values of the matrix elements couple the two different series of vibrations independently of (i) the details of the coupling mechanism or (ii) the polarization investigated. To check this point, we have used $\alpha_1=8\times10^4$ cm^{-2} and computed the oscillator strength of the 799-cm^{-1} E_1-like mode. We get $S=0.04$ which compares well with the experimental value ($S=0.09$) obtained from the oscillator fit. Coming now to the β-to-α distortion, we adjust the oscillator strength of the 396-cm^{-1} E_2-like mode ($S=0.3$) and get $\alpha_2=2.7\times10^{-4}$ cm^{-2}. This gives a quantitative scale of successive perturbations associated with (i) the building of a ring connection in β-quartz and (ii) the change from β to α variety in polarization $\mathbf{E}\perp c$.

Consider now aluminum phosphate and the doubling of the unit cell. Concerning the Γ_2 modes, we have listed our experimental results in Table III. As already said, most of them agree with the results of Ref. 7 (both in strength, energy and broadening), except for the structures found in this work at 375 and 515 cm^{-1}. In both cases they seem to be sample dependent and have not been taken as indicative of a fundamental frequency. (See *Note added in proof.*) However they are too strong to be ignored in any oscillator fit and the corresponding parameters also figure in Table III.

Concerning the LO frequencies precise values have been deduced from Fig. 8(b) and listed in Table III. Please notice again how the magnitude of the longitudinal-transverse splittings supports an assignment in terms of first-order allowed and forbidden B_2-like modes of β-quartz. Moreover, one expects the folded replica to exhibit the smaller (vanishingly small) LO-TO splitting. This is true for the 1160- and 140-cm^{-1} (Γ'_2-like) modes but not for the 440-cm^{-1} one. In this case we find an experimental value (6 cm^{-1}) which compares almost exactly with the one (5 cm^{-1}) obtained for the first-order (B_2-like) mode at 270 cm^{-1}.

We have found it interesting to check how much of our simple model accounts for this apparent discrepancy. We use the same parameter α_1 as we used for SiO_2 and obtained for the B_2-like components $S=0.58$ and 0.07. This is to be compared with 0.23 and 0.17 from the oscillator fit analysis. Next we introduce an additional parameter ϵ which describes the average matrix element $\langle \Gamma_2 \mid D' \mid A_2 \rangle$ when going from α-quartz to berlinite [see Eq. (2)]. We used $\epsilon=1.4\times10^4$ cm^{-2} and computed oscillator strength: 0.007, 0.09, and 0.15 for the 1160-, 440-, and 140-cm^{-1} folded modes, respectively. This compares satisfactorily with the experimental values: 0.010, 0.10, and 0.10, and, taking account of the roughness of the approximation, gives support to our identification of the 440-cm^{-1} phonon mode as a folded replica. The larger activity observed in this case comes from a close resonance effect with the strong A_2-like mode at 490 cm^{-1}.

For the sake of completeness, we have also computed the relative oscillator strengths of the Γ_3-like modes in polarization $\mathbf{E}\perp c$. They have been listed in Table V (column e). Notice again the good overall agreement obtained without the help of any free parameter. We used $S(\text{molecular})=0.7$, $\alpha_1=8\times10^4$ cm^{-2}, $\alpha_2=2.7\times10^{-4}$ cm^{-2}, and $\epsilon=1.4\times10^4$ cm^{-2} and computed values in good agreement with the experimental data. A last point is worth mentioning. From our simple model, we compute oscillator strengths for the missing Γ_3'-like replicas of the order of 0.17 and 0.015, respectively, for the two frequencies expected at 437 and 565 cm^{-1}. This is comparable to (or larger than) the experimental value associated with folded modes effectively detected in our work and marks the limit of our simple model. No quantitative account of the change in symmetry of the wave function is made for dispersive branches and only the resonance effects are taken into account. In the case of the two missing modes, this is the change in the character of the wave function which cancels the polarizability.

VI. CONCLUSION

We have investigated the infrared activity of phonons through the experimental sequence β-SiO_2 to α-SiO_2 and α-$AlPO_4$ and could resolve, for the first time, the folded acoustic mode in polarization $\mathbf{E}\|c$. In polarization $\mathbf{E}\perp c$, two modes appear at low energy the acoustic character of which is assigned to the high-energy component. Some modes, of which the infrared activity is too weak, are missing from the reflectivity spectra and would only ap-

pear in the Raman investigation. Discussing our results in terms of a simple model of infrared-active modes in β-quartz admixed twice, we find a series of coupling coefficients: $\alpha_1 = 8 \times 10^4$ cm^{-2}; $\alpha_2 = 2.7 \times 10^4$ cm^{-2} and $\epsilon = 1.1 \times 10^4$ cm^{-2}, which indicates that the predominant interaction in the whole family is the coupling of the molecular (internal) modes of the tetrahedra to the external ones, whatever are the details of the coupling mechanism.

Note added in proof. Since the completion of this work, an investigation of the off-normal reflectivity spectra of α-$LiIO_3$ and α-quartz has been given by J. L. Duarte and co-workers [Phys. Rev. B **36**, 3368 (1987)]. Analyzing the *s*- and *p*-polarized spectra, both theoretically and experimentally, they could establish that in some cases additional structures appear in the *p* component. They are due to longitudinal modes of a different symmetry and, depending upon their frequency and relative strength, they appear as "dips" or "peaks" in the experimental reflectivity spectra. For instance, this explains the sample-dependent feature noticed in α-quartz at 509 cm^{-1} (see Table II). This should apply as well to any noncubic crystal and we have started new investigations along this line for α-$AlPO_4$. Our preliminary results indicate that, in this way, one can account at least for the extra structure noticed at 515 cm^{-1} in Table III ($\mathbf{E} \| c$ polarization). the corresponding data will be published in a forthcoming paper.

ACKNOWLEDGMENTS

We greatly thank E. Philippot and J. C. Jumas from the Institut de Recherche sur les Matériaux pour l'Electronique for the growth of all α-quartz and aluminum phosphate samples used in this work. We thank also A. Montaner and M. Galtier from the Groupe de Dynamique des Phases Condensées for expert assistance with the use of the Fourier transform spectrometer.

[1]A. Jayaraman, D. L. Wood, and R. G. Maines, Sr., Phys. Rev. B **35**, 8316 (1987).
[2]H. A. A. Sidek, G. A. Saunders, W. Hong, X. Bin, and H. Jianru, Phys. Rev. B **36**, 7612 (1987).
[3]J. F. Scott and P. S. Porto, Phys. Rev. **161**, 903 (1967).
[4](a) W. G. Spitzer and D. A. Kleinman, Phys. Rev. **121**, 1324 (1961); (b) D. A. Kleinman and W. G. Spitzer, Phys. Rev. **125**, 16 (1962).
[5]M. M. Elcombe, Proc. Phys. Soc. London **91**, 947 (1967).
[6]J. F. Scott, Phys. Rev. B **4**, 1360 (1971).
[7]A. N. Lazarev, N. A. Mazhenov, and A. P. Mirgorodskii, Opt. Spectrosc. **46**, 348 (1979).
[8]A. Goullet, J. Camassel, A. Montaner, J. Pascual, J. C. Jumas, and E. Philippot, Phys. Scr. **37**, 395 (1988).
[9]W. Dultz, M. Quicichini, J. F. Scott, and G. Lehmann, Phys. Rev. B **11**, 1648 (1975).
[10]A. Goullet, P. Rouquette, J. Camassel, J. Pascual, and J. C. Jumas, Solid State Commun. **62**, 187 (1987).
[11]F. Matossi, J. Chem. Phys. **17**, 679 (1949).
[12]G. Herzberg, *Infrared and Raman Spectra of Polyatomic Molecules* (Van Nostrand Reinhold, New York, 1945).
[13]J. Pascual, J. Camassel, P. Merle, and H. Mathieu, Phys. Rev. **B21**, 2439 (1980); J. Pascual, J. Camassel, P. Merle, B. Gil, and H. Mathieu, Phys. Rev. B **24**, 2101 (1981).
[14]P. T. T. Wong, F. L. Baudais, and D. J. Moffat, J. Chem. Phys. **84**, 671 (1986).
[15]W. G. Spitzer, D. Kleinman, and D. Walsh, Phys. Rev. **113**, 127 (1959); D. Kleinman and W. G. Spitzer, Phys. Rev. **118**, 110 (1960).
[16]J. Etchepare and M. Merian, J. Chem. Phys. **68**, 533 (1978).
[17]J. B. Bates and A. S. Quist, J. Chem. Phys. **56**, 1528 (1972).
[18]E. E. Russell and E. E. Bell, J. Opt. Soc. Am. **57**, 341 (1967).